

Rethinking Non-idealities in Memristive Crossbars for Adversarial Robustness in Neural Networks

Abhiroop Bhattacharjee, and Priyadarshini Panda
Department of Electrical Engineering, Yale University, USA

Abstract—*Deep Neural Networks* (DNNs) have been shown to be prone to adversarial attacks. With a growing need to enable intelligence in embedded devices in this *Internet of Things* (IoT) era, secure hardware implementation of DNNs has become imperative. Memristive crossbars, being able to perform *Matrix-Vector-Multiplications* (MVMs) efficiently, are used to realize DNNs on hardware. However, crossbar non-idealities have always been devalued since they cause errors in performing MVMs, leading to degradation in the accuracy of the DNNs. Several software-based adversarial defenses have been proposed in the past to make DNNs adversarially robust. However, no previous work has demonstrated the advantage conferred by the non-idealities present in analog crossbars in terms of adversarial robustness. In this work, we show that the intrinsic hardware variations manifested through crossbar non-idealities yield adversarial robustness to the mapped DNNs without any additional optimization. We evaluate resilience of state-of-the-art DNNs (VGG8 & VGG16 networks) using benchmark datasets (CIFAR-10 & CIFAR-100) across various crossbar sizes towards both hardware and software adversarial attacks. We find that crossbar non-idealities unleash greater adversarial robustness ($> 10 - 20\%$) in DNNs than baseline software DNNs. We further assess the performance of our approach with other state-of-the-art efficiency-driven adversarial defenses and find that our approach performs significantly well in terms of reducing adversarial losses.

Index Terms—Deep Neural Networks, Memristive crossbars, Non-idealities, Adversarial robustness



1 INTRODUCTION

In the recent years, resistive crossbar systems have received significant focus for their ability to realize *Deep Neural Networks* (DNNs) by efficiently computing analog dot-products [1], [2], [3]. These systems have been realized using a wide range of emerging technologies such as, *Resistive RAM* (ReRAM), *Phase Change Memory* (PCM) and Spintronic devices [4], [5], [6]. These devices exhibit high on-chip storage density, non-volatility, low leakage and low-voltage operation and thus, enable compact and energy-efficient implementation of DNNs [7], [8].

Despite so many advantages, the analog nature of computation of dot-products in crossbars poses certain challenges owing to device-level and circuit-level non-idealities such as, interconnect parasitics, process variations in the synaptic devices, driver and sensing resistances, etc. [8], [9]. Such non-idealities lead to errors in the analog dot-product computations in the crossbars, thereby adversely affecting DNN implementation in the form of accuracy degradation [10]. Numerous frameworks have been developed in the past to model the impact of non-idealities present in crossbar systems and accordingly, retraining the weights (stored in synaptic devices) of the DNNs to mitigate accuracy degradation [9], [10], [11], [12].

Crossbar-based non-idealities, thus, have so far been devalued because they lead to accuracy degradation in DNNs. However, an interesting aspect of these non-idealities in providing resilience to DNNs against adversarial attacks has been unexplored. DNNs have been shown to be adversarially vulnerable [13]. A DNN can easily be fooled by applying structured, yet, small perturbations on the input, leading to high confidence misclassification of the input.

This vulnerability severely limits the deployment and potential safe-use of DNNs for real world applications such as self-driving cars, malware detection, healthcare monitoring systems etc. [14], [15]. Thus, it is imperative to ensure that the DNN models used for such applications are robust against adversarial attacks. Recent works such as [16], [17] show quantization methods, that primarily reduce compute resource requirements of DNNs, act as a straightforward way of improving the robustness of DNNs against adversarial attacks. A recent work has led to the development of a framework called *QUANOS* that provides a structured method for hybrid quantization of different layers of a DNN to produce energy-efficient, accurate and adversarially robust models [15]. In [15], [16], the authors show that efficiency-driven hardware optimization techniques can be leveraged to improve software vulnerability, such as, adversarial attacks, while yielding energy-efficiency. In this work, we present a comprehensive analysis on how device-level and circuit-level non-idealities intrinsic to analog crossbars can be leveraged for adversarial robustness in neural networks. To the best of our knowledge, we are the first to show that the intrinsic hardware variations manifested through non-idealities in crossbars intrinsically improve adversarial security without any additional optimization. Our main finding is that- *A DNN model mapped on hardware, while suffering accuracy degradation, is also more adversarially resilient than the baseline software DNN.*

Contributions: In summary, the key contributions of this work are as follows:

- We employ a systematic framework in *PyTorch* [18]

to map DNNs onto resistive crossbar arrays and investigate the cumulative impact of various circuit and device-level non-idealities to confer adversarial robustness.

- We analyse the robustness of state-of-the-art DNNs, *viz.* VGG8 and VGG16 [19] using benchmark datasets- CIFAR-10 and CIFAR-100 [20], respectively, across various crossbar dimensions.
- We show that crossbar-based non-idealities impart robustness in neural networks against both hardware and software-based adversarial attacks.
- We find that non-idealities lead to higher adversarial robustness ($> 10 - 20\%$ for both FGSM and PGD-based adversarial attacks on hardware) in DNNs mapped onto resistive crossbars than DNNs evaluated on software.
- We investigate the role of various crossbar parameters (such as R_{MIN}) in unleashing adversarial robustness to DNNs mapped onto crossbars. We also study the impact of input *Pixel Discretization* proposed in [16] together with crossbar non-idealities on adversarial robustness.
- A comparison of our proposed method with other state-of-the-art quantization techniques is also presented to emphasise the importance of hardware non-idealities in imparting resilience to DNNs against adversarial inputs.

2 RELATED WORKS

2.1 Strategies to map DNNs onto crossbars with non-idealities for inference

Prior research works have focused on modeling crossbar non-idealities to mitigate the problem of accuracy degradation incurred when DNNs are mapped onto them. Several frameworks have been proposed such as, *CxDNN* [10], that employs matrix-inversion techniques combined with *Kirchoff's circuit laws* to model the effect of interconnect parasitics and peripheral non-idealities in the resistive crossbar arrays. The authors in [21] have presented an approximation technique based on sample input/output behavior. However, these analytical models take into account only linear data-dependent non-idealities while modeling the crossbar instances. Recent frameworks such as *GenieX* [9] use a neural network-based approach to accurately encapsulate the effects of both data dependent and non-data dependent non-idealities and assess their impact on accuracy degradation. *PUMA* is the first *Instruction Set Architecture* (ISA)-programmable inference accelerator based on hybrid CMOS-memristor crossbar technology, which is designed to maintain crossbar area and energy efficiency as well as storage density. *PUMA* has been shown to outperform other state-of-the-art CPUs, GPUs, and ASICs for ML acceleration [7], [22], [23], [24]. Nevertheless, none of the aforementioned techniques or architectures have helped understand the advantages that the intrinsic non-idealities of the crossbar structures may confer in terms of adversarial robustness to DNNs.

2.2 Adversarial Defenses

In the recent years, several heuristic adversarial defense strategies have been developed, including adversarial training [13], [25], [26], [27], [28], randomization-based techniques [29], [30], [31] and denoising methods [32], [33], [34], [35]. However, these defenses might be broken by a new attack in the future since they lack a theoretical error-rate guarantee [36]. Hence, researchers have strived to develop certified defensive methods [37], [38], [39], [40], which always maintain a certain accuracy under a well-defined class of attacks [36]. Even though the certified defense methods indicate a way to reach theoretically guaranteed security, their accuracy and efficiency are far from meeting the practical requirements [36]. Apart from these, several quantization-based methods on software have been proposed of late, including works like [15], [16], [17] to improve resilience of neural networks against adversarial perturbations. The work in [16] deals with discretization of the input space (or allowed pixel levels from 256 values or 8-bit to 4-bit, 2-bit). It shows that input discretization improves the adversarial robustness of DNNs for a substantial range of perturbations, besides improvement in its computational efficiency with minimal loss in test accuracy. Likewise, *QUANOS* [15] is a framework that performs layer-specific hybrid quantization of DNNs based on a metric termed as *Adversarial Noise Sensitivity* (ANS) to make DNNs robust against adversarial perturbations. In contrast to prior works, we present a first of its kind work that comprehensively studies the inherent advantage of hardware non-idealities towards imparting adversarial robustness to DNNs without relying upon other software-based optimization methodologies. Note, we also show that combining previously proposed optimization strategies, such as pixel discretization, with analog crossbars further improves robustness.

3 BACKGROUND

3.1 Adversarial Attacks

DNNs are vulnerable to adversarial attacks in which the model gets fooled by applying precisely calculated small perturbations on the input, leading to high confidence misclassification [15]. The authors in [25] have proposed a method called *Fast Gradient Sign Method* (FGSM) to generate the adversarial input by linearization of the loss function (L) of the trained models with respect to the input (X) as shown in equation (1).

$$X_{adv} = X + \epsilon \times \text{sign}(\nabla_x L(\theta, X, y_{true})) \quad (1)$$

Here, y_{true} is the true class label for the input X ; θ denotes the model parameters (weights, biases etc.) and ϵ quantifies the degree of distortion.

The quantity $\Delta = \epsilon \times \text{sign}(\nabla_x L(\theta, X, y_{true}))$ is the net perturbation added to the input (X), which is controlled by ϵ . It is noteworthy that gradient propagation is, thus, a crucial step in unleashing an adversarial attack. Furthermore, the contribution of gradient to Δ would vary for different layers of the network depending upon the activations [15]. In addition to FGSM-based attacks, multi-step variants of FGSM, such as *Projected Gradient Descent* (PGD) [13] have also been proposed that cast stronger attacks.

To build resilience against against small adversarial perturbations, defense mechanisms such as gradient masking or obfuscation [41] have been proposed. Such methods construct a model devoid of useful gradients, thereby making it difficult to create an adversarial attack.

Types of Attacks: Broadly, attacks to evaluate adversarial robustness are classified as: *Black-Box* (BB) and *White-Box* (WB). WB attacks are launched when the attacker has complete knowledge of the target model parameters and training information. BB attacks, on the other hand, are launched when the attacker has no knowledge about the target model parameters. Resilience against WB adversaries also guarantees resilience against the BB ones for similar perturbation (ϵ) range [15]. Thus, all our subsequent experiments are based on WB adversaries for the assessment of adversarial robustness.

In this work, *Clean Accuracy* (*CA*) refers to the accuracy of a DNN when presented with the test dataset in absence of an adversarial attack. We define *Adversarial Accuracy* (*AA*) as the accuracy of a DNN on the adversarial dataset created using the test data for a given task. *Adversarial Loss* (*AL*) is defined as the difference between *CA* and *AA*, i.e., $AL = CA - AA$. Higher the value of *AA*, smaller will be the value of *AL*, which implies increased robustness against adversarial attacks.

3.2 Resistive crossbar arrays and their non-idealities

Resistive crossbar arrays can be harnessed to implement *Matrix-Vector-Multiplications* (MVMs) in an analog manner. Crossbars (Fig. 1(a)) consist of 2D arrays of synaptic devices (programmable resistors realized using emerging nanotechnologies), *Digital-to-Analog* (DAC), and *Analog-to-Digital* (DAC) converters and a write circuit. The synaptic devices at the intersection of each row and column are configured to a particular value of conductance (that ranges from G_{MIN} to G_{MAX}), by enabling the corresponding write circuits along the *Write Wordline* (WWL) and the *Bitline* (BL). Thereafter, the MVMs are performed by converting the digital inputs to analog voltages on the *Read Wordlines* (RWLs) using DACs, and sensing the output current flowing through the bitlines (BLs) using the ADCs [8].

Equation (2) shows the ideal MVM operation for an $M \times N$ crossbar, for which V_{in} is a $1 \times M$ vector comprising the input analog voltages, G_{ideal} is the $M \times N$ conductance matrix (formed by mapping the weights of a DNN onto the crossbar instances), and $I_{out_{ideal}}$ is a $1 \times N$ vector comprising output currents.

$$I_{out_{ideal}} = V_{in} * G_{ideal} \quad (2)$$

Non-idealities: The analog nature of the computation leads to various non-idealities resulting in errors in the MVMs. These include device-level and circuit-level non-idealities in the resistive crossbars. Fig. 1(b) shows the equivalent circuit for the crossbar array and its peripherals accounting for the non-idealities listed in TABLE 1. The circuit-level non-idealities have been modelled as parasitic resistances. The cumulative effect of all the non-idealities results in the deviation of the output current from its ideal value, resulting in an $I_{out_{non-ideal}}$ vector. The relative

TABLE 1
Various circuit-level and device-level non-idealities in a resistive crossbar array

Type of non-idealities	Parameters
Circuit non-idealities	Rdriver, Rwire_row, Rwire_col, Rsense
Device non-idealities	Gaussian variation profile

deviation of $I_{out_{non-ideal}}$ from its ideal value is denoted by *non-ideality factor* (NF) [9] such that:

$$NF = (I_{out_{ideal}} - I_{out_{non-ideal}}) / I_{out_{ideal}} \quad (3)$$

Thus, increased non-idealities in crossbars can induce a greater value of NF. This can lead to a significant impact on the computational accuracy of crossbars and therefore, degradation in the accuracy of the DNNs implemented on hardware [8], [9], [10].

Crossbar Mapping: In this work, we use a similar procedure as that of [8], [10] for mapping DNNs onto crossbars of various dimensions as shown in Fig. 3(b). First, the weights of each layer of the DNN are partitioned based on the size of the crossbar array used and mapped onto the crossbar instances. Thereafter, the corresponding conductance for each value of DNN weight in a crossbar instance is computed by taking into account the synaptic device parameters, viz. G_{MIN} , G_{MAX} and bit-precision. This gives us the ideal conductance matrix (G_{ideal}). Finally, we consider the circuit-level and device-level non-idealities present in a crossbar instance specified in TABLE 1, and convert G_{ideal} into $G_{non-ideal}$ using circuit laws (*Kirchoff's laws* and *Ohm's law*) and linear algebraic operations [8]. This completes the mapping of the weights of the DNN onto the crossbar instances.

3.3 Can non-idealities be leveraged for adversarial robustness?

Non-idealities inherent in crossbars have so far been projected in a negative light since, they lead to degradation in clean accuracy when DNNs are mapped onto them. However, in this work, we show how the non-idealities (or an increased value of NF for a crossbar) lead to robustness of DNNs against adversarial attacks. Thus, we observe lower adversarial loss (*AL*) with respect to the corresponding software implementation of the DNNs. *We argue that non-idealities intrinsically lead to defense via gradient obfuscation against adversarial perturbations since gradient propagation, as discussed in Section 3.1, is crucial to initiate an adversarial attack.*

Fig. 2 pictorially demonstrates the intuition behind creation of an adversary in DNNs and how hardware non-idealities can cause gradient obfuscation. DNNs, being discriminative models, partition a very high-dimensional input space into different classes by learning appropriate decision boundaries. The class-specific decision boundaries simply divide the space into hyper-volumes. These hypervolumes consist of the training data examples as well as large areas of unpopulated space that is arbitrary and untrained. The decision boundary during model training extrapolates to vast regions of unpopulated high-dimensional subspace because of linearity/generalization in the model behavior.

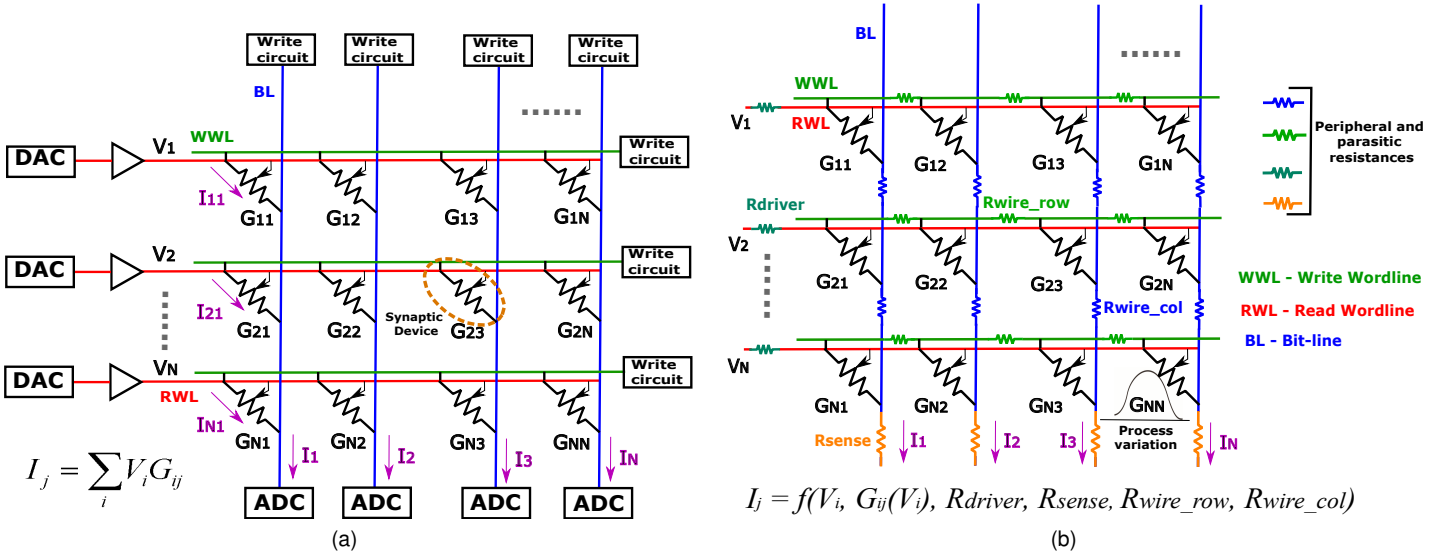


Fig. 1. (a) An ideal crossbar array; (b) A typical non-ideal crossbar array structure with resistive circuit-level non-idealities

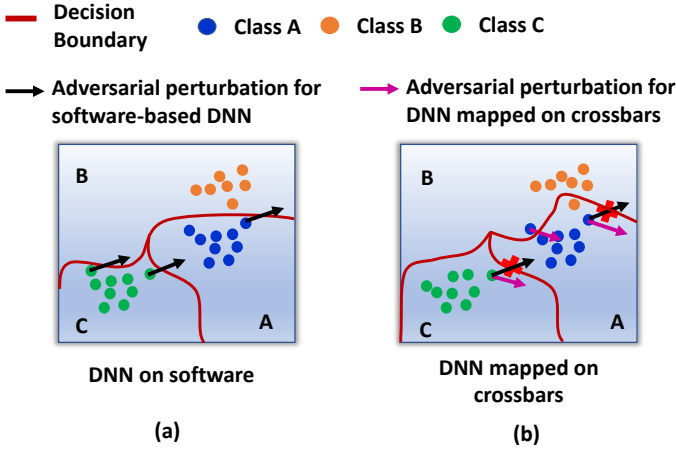


Fig. 2. Pictorial depiction of creation of adversaries for software and hardware-based DNNs - (a) The data points (shown as 'dots') encompass the data manifold in the high-dimensional subspace. The classifier is trained to separate the data into different classes or hypervolumes based on which the decision boundary is formed. Adversaries are created by perturbing the data points into these empty regions or hypervolumes and are thus misclassified; (b) The decision boundaries get shifted owing to the crossbar-based non-idealities in hardware, resulting in the placement of certain data points into a different hypervolume leading to accuracy degradation. However, due to gradient obfuscation owing to crossbar non-idealities, many data points remain restricted in their original hypervolumes on perturbations. This results in better adversarial robustness in hardware-based DNNs.

But this exposes the model to adversarial attacks [16]. Adversarial perturbations, essentially, can shift a data point from its typical hypervolume region to another, leading to high-confidence misclassification. This has been shown in Fig. 2(a) with black arrows for a DNN evaluated on software.

However, when a DNN is mapped onto crossbar arrays, the decision boundaries are shifted owing to the crossbar-based non-idealities, resulting in the placement of certain data points into a different hypervolume (Fig. 2(b)). This leads to misclassifications and hence, degradation in the

clean accuracy of the DNN. Also, on unleashing adversarial attacks on a DNN mapped on crossbars, the displacement of a data point in the high-dimensional subspace gets altered in a different direction. This has been marked in Fig. 2(b) using violet arrows which demarcate another direction *w.r.t.* the one demarcated using black arrows (for DNNs evaluated on software). Thus, instead of moving into a different hypervolume, the many perturbed data points remain restricted in their original hypervolumes, thereby resulting in lower adversarial losses (ALs) for the DNN and greater adversarial robustness.

Quantifying the intuition in Fig. 2: To support our gradient obfuscation argument, let us consider a DNN mapped onto crossbars as f . The net perturbation added to the input (X) in case of an adversarial attack is given by $\Delta = \epsilon \times \text{sign}(\nabla_x L(\theta, X, y_{true}))$ (refer to Section 3.1). Without loss of generality, we assume the loss function (L) from the hardware mapped DNN to be a function of the output current emerging out of a crossbar array (I_{out}), *i.e.*:

$$L = f(I_{out})$$

Since DNNs are sufficiently linear owing to the ReLU activation functions being used, we can assume that:

$$L \approx I_{out}$$

In the ideal scenario of crossbars with no non-idealities,

$$L \approx I_{out_{ideal}}$$

which implies,

$$\Delta_{ideal} = \epsilon \times \text{sign}(\nabla_x(I_{out_{ideal}})) \quad (4)$$

However, in the case of non-idealities being present in crossbar structures,

$$I_{out_{non-ideal}} = I_{out_{ideal}} - \gamma$$

where, γ denotes the deviation of the output current of the crossbar from its ideal value due to the inherent non-idealities. Hence, in the non-ideal scenario, we have:

$$\Delta_{non-ideal} = \epsilon \times \text{sign}(\nabla_x(I_{out_{ideal}} - \gamma)) \quad (5)$$

From equation (5), we find that there is a deviation in the adversarial perturbation from its ideal value owing to crossbar non-idealities. Hence, this explains the reason behind an altered displacement of data points in the high-dimensional subspace *w.r.t.* the direction of displacement in case of a DNN evaluated on software (Fig. 2(b)).

In this work, we employ a framework in *PyTorch* similar to *RxNN* [8], to map DNNs onto a resistive crossbar array and investigate the cumulative impact of the circuit and device-level non-idealities (mentioned in TABLE 1) on the robustness of neural networks against adversarial inputs.

4 METHODOLOGY

The methodology described in Fig. 3(a) is adopted to assess the robustness of DNNs against adversarial inputs when implemented on hardware. The entire process is divided into two parts:

4.1 Part-1 for Software DNN:

We employ benchmark datasets- CIFAR-10 and CIFAR-100 to evaluate VGG8 and VGG16 networks, respectively. These networks are first trained on PyTorch with the appropriate training datasets. Subsequently, we obtain two kinds of trained models as follows:

- 1) **Model-1:** A standard model trained without adding any random noise to its activations.
- 2) **Model-2:** A model trained with random noise added to all neuronal activation values. Such noise enabled training has been used in past works [42] to mitigate the accuracy degradation observed from mapping DNNs onto crossbars. Essentially, adding random noise to the neuronal activations is a crude and approximate way of modeling non-idealities during the training process.

Attack-SW: We launch FGSM and PGD attacks on the software models by adding adversarial perturbations to the clean test inputs. We record the adversarial accuracies (AAs) and adversarial losses (ALs) in case of each attack.

4.2 Part-2 for Crossbar mapped DNN:

Using a PyTorch-based framework, we layer-wise map the software DNN weights separately for both Model-1 and Model-2 onto resistive crossbar instances of sizes- 16x16, 32x32 and 64x64 respectively. We follow the procedure of mapping the weights of the DNN onto crossbars as described in Section 3.2.

We calculate the CAs for both *Model-1* and *Model-2* for the crossbar mapped DNN, which are expected to be lesser than the values obtained for software DNN. Thereafter, we launch FGSM and PGD attacks on the mapped crossbar-based models in two modes termed as:

- 1) **Attack-1:** The adversarial perturbations for each attack, FGSM & PGD, are created using the software-based DNN model’s loss function and then added to the clean input that yields the adversarial input. The generated adversaries are then fed to the crossbar mapped DNN to monitor *AL*.

TABLE 2
Parameters and their values associated with a resistive crossbar array

Parameter	Value
Rdriver	1 $k\Omega$
Rwire_row	5 Ω
Rwire_col	10 Ω
Rsense	1 $k\Omega$
R_{MIN}	20 $k\Omega$
R_{MAX}	200 $k\Omega$

- 2) **Attack-2:** The adversarial inputs are generated for each attack, FGSM & PGD, using the loss from the crossbar-based hardware models. As a result, we can expect the adversaries in this case will not be as strong as *Attack-1* adversaries owing to the presence of non-idealities that can interfere in the attack generation process.

We finally record the adversarial accuracies (AAs) and adversarial losses (ALs) for all modes: *Attack-SW*, *Attack-1*, *Attack-2*.

5 RESULTS AND DISCUSSION

5.1 Comparison with clean accuracies

The parameters pertaining to the non-ideal resistive crossbars for mapping the DNNs are listed in TABLE 2 and employed for all the simulations unless stated otherwise. Also, device-level process variation shown in experiments below has been modelled as a Gaussian variation in the resistances of the synaptic devices with $\sigma/\mu = 10\%$.

Fig. 4 presents a comparison of clean accuracies of the trained VGG8 and VGG16 networks (note, *Model-1* type) when evaluated on software and after mapping on non-ideal crossbars of various dimensions (excluding the device-level variations). It can be observed that the clean accuracies drop post-mapping on the crossbars which is a direct implication of the inherent non-idealities in a crossbar causing errors in MVMs as discussed in Section 3.2. We also see that accuracies drop more for larger sized crossbars. In the subsequent subsections, we discuss the implications on adversarial robustness by inducing *Attack-1* and *Attack-2* on the crossbar-mapped models.

5.1.1 Results with CIFAR-10 dataset

In Fig. 5, it can be observed that *AL* in case of an FGSM attack on the DNNs mapped onto crossbars of various dimensions (16x16, 32x32, 64x64) are lesser than that of a DNN evaluated on software. For different attack strengths quantified by ϵ values, the value of *AL* in case of *Attack-SW* is significantly greater than *Attack-1* or *Attack-2* ($> 10-15\%$). In other words, the hardware-based non-idealities that come into play when DNNs are mapped onto crossbars provide robustness against adversarial inputs.

PGD attack, being a multi-step variant of FGSM attack, is much stronger and yields significantly higher adversarial losses in DNNs than FGSM attacks. Similar to the case of FGSM attacks, non-idealities in crossbars provide robustness to the mapped DNNs against adversarial inputs as shown in Fig. 6.

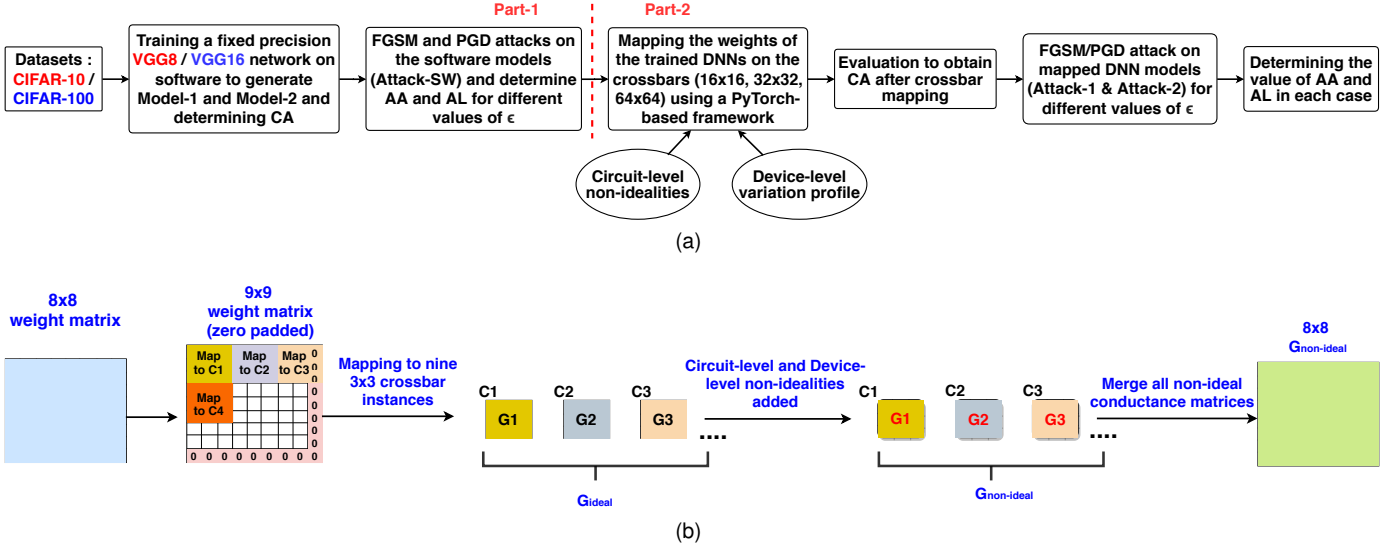


Fig. 3. (a) Flow diagram explaining the methodology followed (CIFAR-10 dataset is used with a VGG8 network (highlighted in red) while, CIFAR-100 dataset is used with a VGG16 network (highlighted in blue)); (b) Pictorial depiction of the steps associated with mapping of an 8x8 weight matrix into crossbar instances of size 3x3

TABLE 3

Table showing AL (%) for different values of ϵ in case of Attack-2 (PGD) on crossbar sizes of 16x16, 32x32 and 64x64 on Model-1 and Model-2 of VGG8 network with CIFAR-10 dataset

ϵ	Attack-2 (PGD) on Model-1					Attack-2 (PGD) on Model-2				
	2/255	4/255	8/255	16/255	32/255	2/255	4/255	8/255	16/255	32/255
Cross16	71.78	71.89	71.97	72.52	73.92	68.9	69	69.06	69.5	70.46
Cross32	71.13	71.22	71.55	71.97	73.36	68.77	68.79	69.01	69.41	70.3
Cross64	67.92	67.14	67.38	68.73	71.06	68.43	68.56	68.76	69.15	70.07

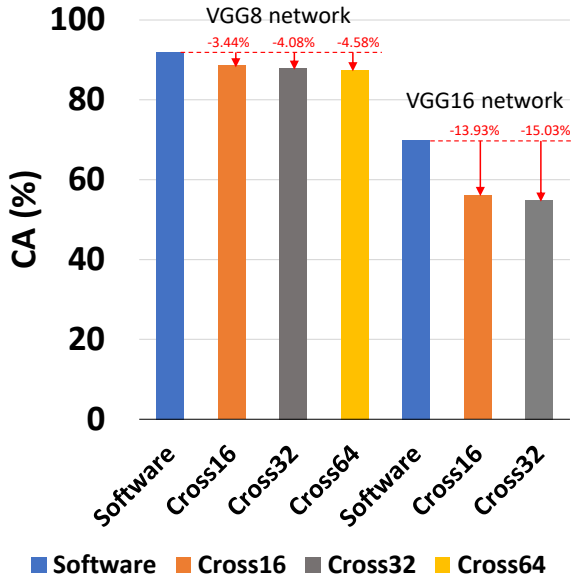


Fig. 4. Bar diagram showing CA of a VGG8 and VGG16 networks on software and crossbars of sizes 16x16, 32x32 and 64x64

For both FGSM and PGD attacks, we find that ALs in case of Attack-2 are lesser than Attack-1, indicating that the mapped DNNs are more resilient to adversarial perturbations created using the crossbar-based hardware models

than the software-based perturbations. Interestingly, we also find that larger crossbar sizes provide greater robustness against adversarial attacks (characterized by lower values of AL for the same value of ϵ) than the smaller ones. This is because larger crossbars involve greater number of parasitic components (non-idealities), thereby imparting more robustness. This has been shown in TABLE 3 where, the crossbar size of 64x64 provides the best robustness among the other crossbar sizes.

Fig. 7 shows the variation in the CAs of Model-1 and Model-2 for both baseline software DNN (VGG8 network) and when mapped onto crossbars. We find that on training a DNN with random noise added to its activations (Model-2), CAs are significantly lower than those for a normal DNN (Model-1). As already discussed in the case of Model-1, we observe similar results for both FGSM and PGD attacks on Model-2 shown in TABLE 4 and TABLE 5, all of which affirm that hardware-based non-idealities lead to reduction in adversarial losses and improvement in adversarial robustness (> 10 – 15%). Furthermore, in case of Model-2, we also find that larger crossbar sizes provide greater robustness against adversarial attacks than the smaller ones as indicated by TABLE 3, where AL for a particular value of ϵ is the highest in case of a 16x16 crossbar, followed by a 32x32 crossbar and the least for a 64x64 crossbar. From the values of AL presented in TABLE 3, the reader might be misled into thinking that Model-2 yields greater adversarial robustness than Model-1 when mapped on crossbars.

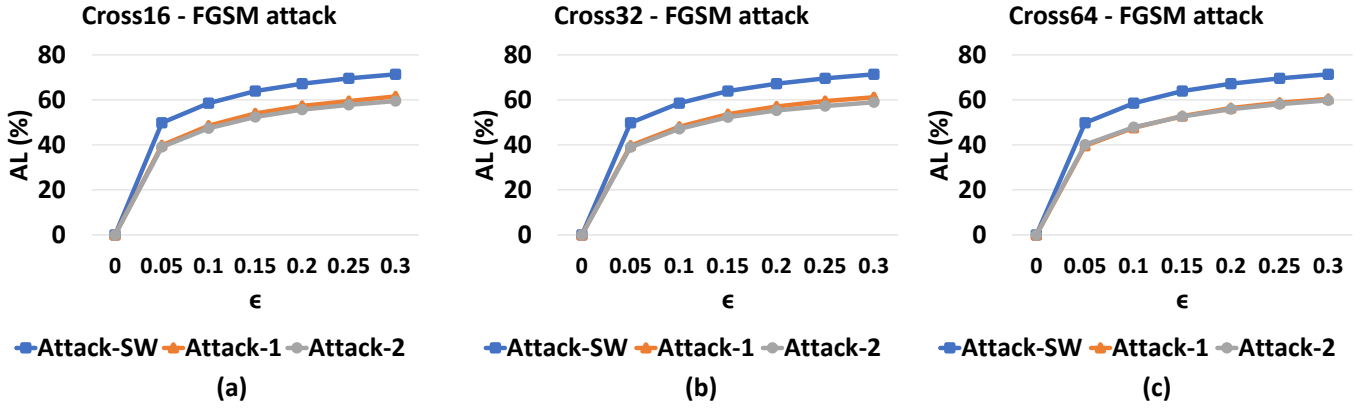


Fig. 5. A plot between AL and ϵ for Attack-SW, Attack-1 and Attack-2 (FGSM) on Model-1 (VGG8 network with CIFAR-10 dataset) for crossbar sizes - (a) 16x16; (b) 32x32; (c) 64x64

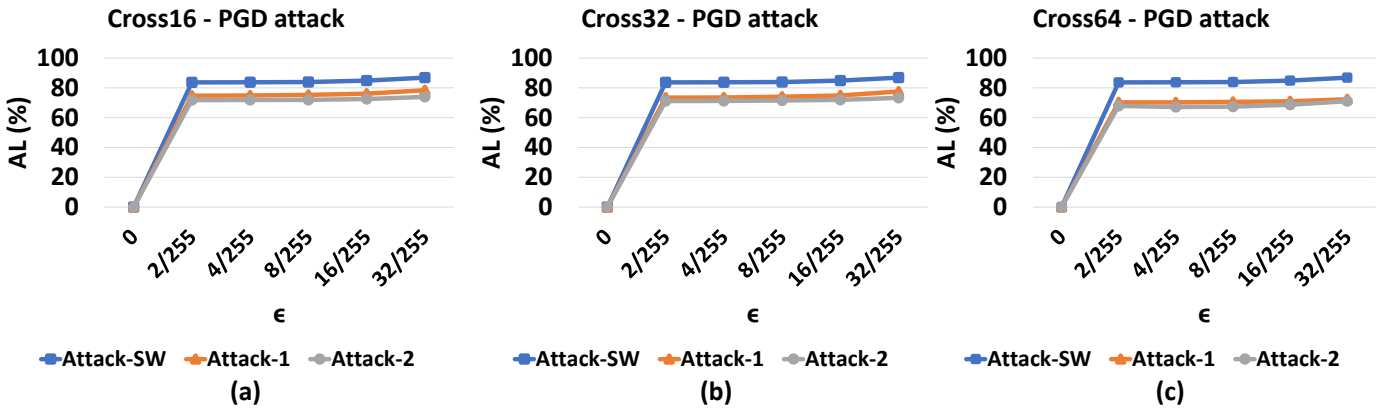


Fig. 6. A plot between AL and ϵ for Attack-SW, Attack-1 and Attack-2 (PGD) on Model-1 (VGG8 network with CIFAR-10 dataset) for crossbar sizes - (a) 16x16; (b) 32x32; (c) 64x64

TABLE 4

Table showing AL (%) for different values of ϵ in case of Attack-SW, Attack-1 and Attack-2 (FGSM) on Model-2 (VGG8 network with CIFAR-10 dataset) for crossbar sizes of 16x16 and 32x32

ϵ	16x16 crossbar							32x32 crossbar						
	0	0.05	0.1	0.15	0.2	0.25	0.3	0	0.05	0.1	0.15	0.2	0.25	0.3
Attack-SW	0	53.52	62.86	68.5	71.64	74.03	75.37	0	53.52	62.86	68.5	71.64	74.03	75.37
Attack-1	0	39.67	48.32	53.38	56.68	59.08	60.73	0	39.93	48.51	53.27	56.59	58.75	60.29
Attack-2	0	38.08	46.08	50.49	53.45	54.99	56.44	0	38.44	45.6	50.5	53.01	54.75	56.05

However, the fact is that the general trend of finding lower values of AL for Model-2 with respect to Model-1 for a given ϵ is because of significantly smaller CAs of Model-2 when compared with Model-1 (Fig. 7), and not higher values of AA.

Effect of R_{MIN} on adversarial robustness: The effective resistance of a crossbar structure is the parallel combination of resistances along its rows and columns. A smaller value of R_{MIN} reduces the effective resistance of the crossbar and increases the value of NF for the crossbar [9]. As we have already argued that an increased value of NF improves the adversarial robustness of crossbars, so on decreasing R_{MIN} to $10 k\Omega$ (maintaining a constant R_{MAX}/R_{MIN} ratio of 10) we find that ALs (for a PGD attack) in case of smaller R_{MIN} are lower than the corresponding ALs for a larger R_{MIN} as

shown in Fig. 8.

However, we also observe that in case of smaller R_{MIN} , the DNN achieves greater robustness against Attack-1 than Attack-2, contrary to what has been observed in Fig. 5 and Fig. 6. This is because of larger adversarial perturbations created on hardware during Attack-2 with lower R_{MIN} . Lowering R_{MIN} causes larger values of output currents in the crossbar arrays (due to smaller effective resistance of the crossbars). To verify this, we employ a metric called *Distortion Coefficient* (d) that quantifies the degree of distortion of test images of the dataset over a batch during an adversarial attack. Mathematically, it is given as:

$$d = \frac{\sum_i |NC - NA|}{N} \quad (6)$$

TABLE 5

Table showing AL (%) for different values of ϵ in case of Attack-SW, Attack-1 and Attack-2 (PGD) on Model-2 (VGG8 network with CIFAR-10 dataset) for crossbar sizes of 16x16 and 32x32

16x16 crossbar							32x32 crossbar					
ϵ	0	2/255	4/255	8/255	16/255	32/255	0	2/255	4/255	8/255	16/255	32/255
Attack-SW	0	81.25	81.33	81.5	82.34	84.16	0	81.25	81.33	81.5	82.34	84.16
Attack-1	0	72.57	72.6	73.11	73.78	75.38	0	72.01	72.26	72.51	73.41	75.08
Attack-2	0	68.9	69	69.06	69.5	70.46	0	68.77	68.79	69.01	69.41	70.3

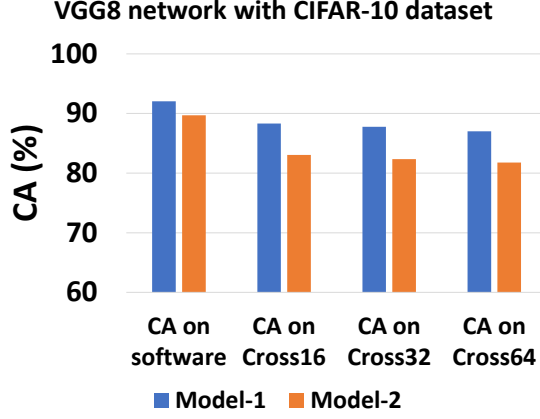


Fig. 7. Comparison of CAs of VGG8 network (software-based as well as crossbar-mapped) for Model-1 and Model-2 using CIFAR-10 dataset

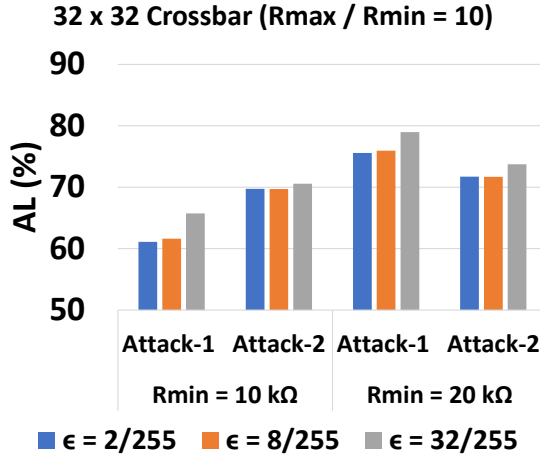


Fig. 8. Bar-diagram showing ALs in case of Attack-1 and Attack-2 (PGD) for a VGG8 network mapped on 32x32 crossbars using CIFAR-10 dataset for two different values of R_{MIN} at constant R_{MAX}/R_{MIN} ratio

where, NC = normalized pixel value of clean image, NA = normalized pixel value of adversarially perturbed image, i denotes the indices of a pixel in an image and N = total number of pixels across an image.

From TABLE 6, we observe that the distortion coefficient d over a batch of images for Attack-2 is greater than Attack-1. This verifies that Attack-2 is stronger than Attack-1 and hence, greater adversarial robustness is observed in case of Attack-1 w.r.t Attack-2 with lower R_{MIN} .

Effect of R_{MAX} at constant R_{MIN} on adversarial robustness: Fig. 9 shows results for PGD attack on a VGG8 network mapped onto crossbars with constant R_{MIN} of

TABLE 6

Table showing values of distortion coefficient over a batch (calculated using equation 6) and AL for PGD attack ($\epsilon = 8/255$) on VGG8 network mapped onto 32x32 crossbar with CIFAR-10 dataset. The value of $R_{MIN} = 10 k\Omega$ and $R_{MAX}/R_{MIN} = 10$ for the crossbar

Type of Attack	Distortion coefficient (d)	AL (%)
Attack-1	0.047288	61.61
Attack-2	0.050654	69.72

20 $k\Omega$ and R_{MAX}/R_{MIN} ratio increased by increasing the value of R_{MAX} . We find that even increasing R_{MAX} by a factor of 200 results in no added advantage in terms of adversarial robustness for Attack-1 or Attack-2. Hence, we find that there is a greater impact of R_{MIN} on adversarial robustness than R_{MAX} .

Effect of process variation on adversarial robustness:

Fig. 10 shows results for PGD attack on a VGG8 network mapped onto crossbars by varying the σ/μ ratio, pertaining to synaptic device variation, from 5 – 15%. Similar to the case of increasing the value of R_{MAX} , we find no added advantage in terms of adversarial robustness for Attack-1 or Attack-2 by increasing the Gaussian variation in the devices of the crossbars.

Studying the combined effect of input pixel discretization and crossbar non-idealities: In [16], the authors show that input pixel discretization from 256 or 8-bit level to 4-bit, 2-bit improves adversarial resilience of software DNNs. Here, we unleash FGSM attack on the VGG8 network mapped onto 32x32 crossbars with input image pixels of the CIFAR-10 test dataset discretized to 4-bits (or 16 levels) and 2-bits (4 levels). The results are shown in Fig. 11. Interestingly, we find that with pixel discretization, ALs on crossbar mapped DNN for both Attack-1 and Attack-2 attain a fixed value and do not vary on increasing ϵ from 0.1 to 0.3. This implies that input pixel discretization does not necessarily help in resiliency when attacking hardware mapped DNNs. For lower values of ϵ , greater adversarial robustness is observed without pixel discretization. At higher value of ϵ ($\epsilon = 0.3$), the combined effect of 4-bit pixel discretization and crossbar non-idealities outperforms the rest in terms of adversarial robustness. Furthermore, 2-bit pixel discretization not only reduces the clean accuracy to 72.89% but also imparts marginally lesser adversarial robustness than 4-bit pixel discretization - < 0.8% for Attack-1 and < 1.48% for Attack-2.

5.1.2 Results with CIFAR-100 dataset

The results shown in Fig. 12 are similar to those in the case of the VGG8 network evaluated with CIFAR-10 dataset.

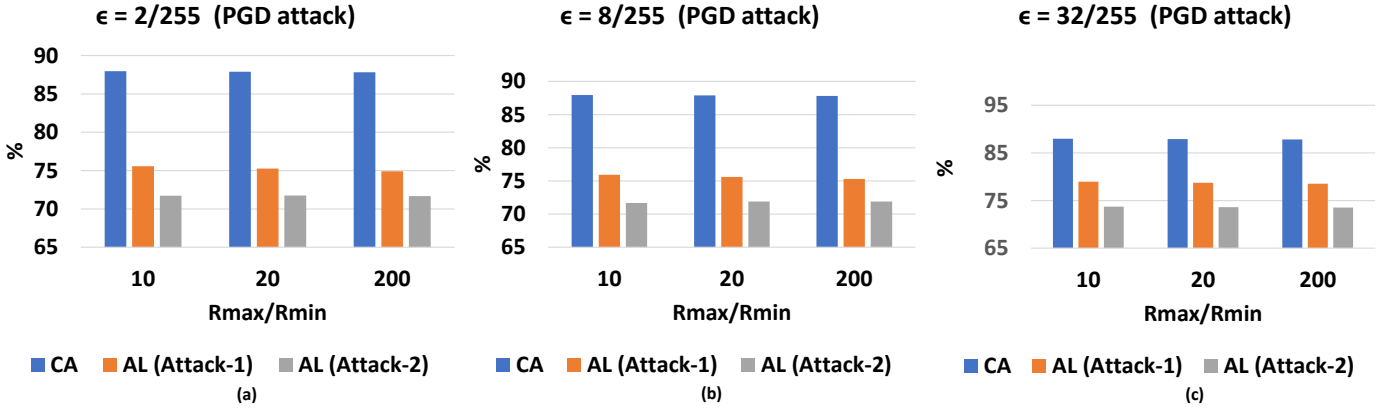


Fig. 9. Bar-diagram showing CAs and ALs (for PGD-based *Attack-1* and *Attack-2*) for a VGG8 network mapped on 32x32 crossbars using CIFAR-10 dataset for different values of R_{MAX} with - (a) $\epsilon = 2/255$; (b) $\epsilon = 8/255$; (c) $\epsilon = 32/255$

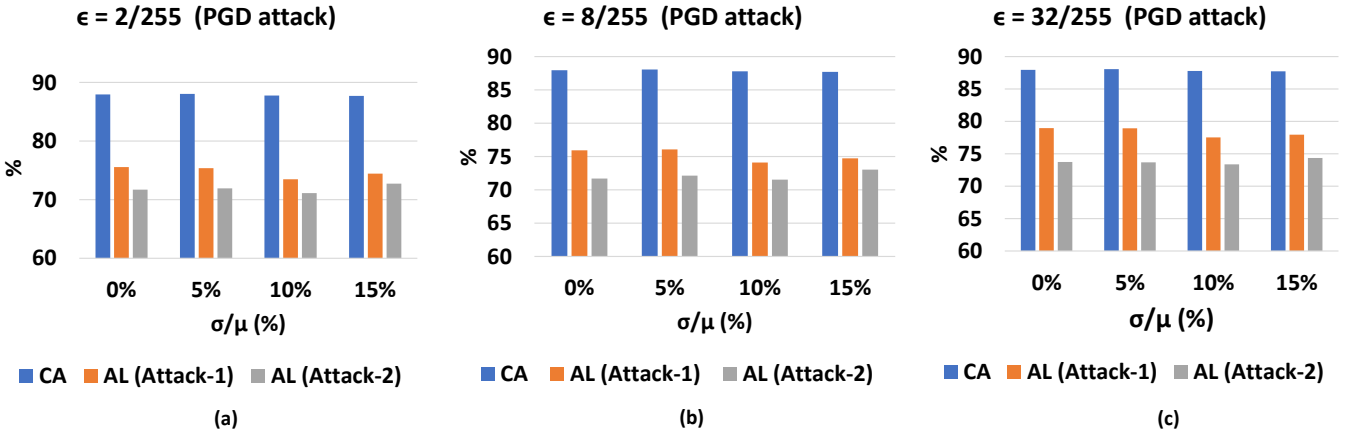


Fig. 10. Bar-diagram showing CAs and ALs (for PGD-based *Attack-1* and *Attack-2*) for a VGG8 network mapped on 32x32 crossbars using CIFAR-10 dataset for different values of σ/μ (synaptic device variation) with - (a) $\epsilon = 2/255$; (b) $\epsilon = 8/255$; (c) $\epsilon = 32/255$

Crossbar-based non-idealities impart adversarial robustness to the mapped VGG16 network ($> 10 - 20\%$) against both FGSM and PGD-based attacks. However, with CIFAR-100 dataset, we clearly observe that DNN shows greater adversarial robustness against PGD attack in case of *Attack-2* w.r.t *Attack-1* than what is observed with CIFAR-10 dataset. Quantitatively, there is $\sim 7\%$ greater robustness in case of *Attack-2* w.r.t *Attack-1* with CIFAR-100 dataset against $\sim 4\%$ with CIFAR-10 dataset, albeit the drop in clean accuracy for the DNN mapped onto crossbars is higher in case of CIFAR-100 dataset (Fig. 4).

Comparison with Related works: We compare the performance of non-ideality-driven adversarial robustness in crossbars against state-of-the-art software-based adversarial techniques described in [15], [16]. Note, [15], [16] use efficiency driven transformations (that *implicitly* translate to hardware benefits) such as, quantization to improve resilience. In contrast, our work utilizes *explicit* hardware variations to improve robustness. We aim to compare the robustness obtained from implicit and explicit hardware techniques. We observe that for single-step FGSM attack on a VGG16 network mapped on 32x32 crossbars (note, Model-1 type DNN), adversarial robustness due to crossbar non-idealities, *Attack-1* results, outperforms all other tech-

niques (Fig. 13(a)). For multi-step PGD attack, *Attack-1* ranks second ((Fig. 13(b)). With respect to 4-bit (4b) *pixel discretization* of input data [16], non-idealities in crossbars impart $\sim 15\%$ greater adversarial robustness in case of FGSM attack and $\sim 12\%$ greater adversarial robustness in case of PGD attack. On the other hand, in case of FGSM attack, crossbar-based non-idealities impart $\sim 4\%$ greater adversarial robustness than QUANOS [15], while for PGD attack, QUANOS outperforms by $\sim 18 - 22\%$.

6 CONCLUSION

In this work, we perform a comprehensive analysis to show how crossbar-based non-idealities can be harnessed for adversarial robustness. This work brings in a new standpoint that does not devalue the importance of non-idealities or parasitics present in crossbar systems. We develop a framework based on *PyTorch* that maps state-of-the-art DNNs (VGG8 and VGG16 networks) onto resistive crossbar arrays and evaluates them with benchmark datasets (CIFAR-10 and CIFAR-100). We show that circuit-level non-idealities (e.g., interconnect parasitics) and synaptic device-level non-idealities intrinsically provide robustness to the mapped DNNs against adversarial attacks, such as FGSM and PGD attacks. This is reflected by lower accuracy degradations

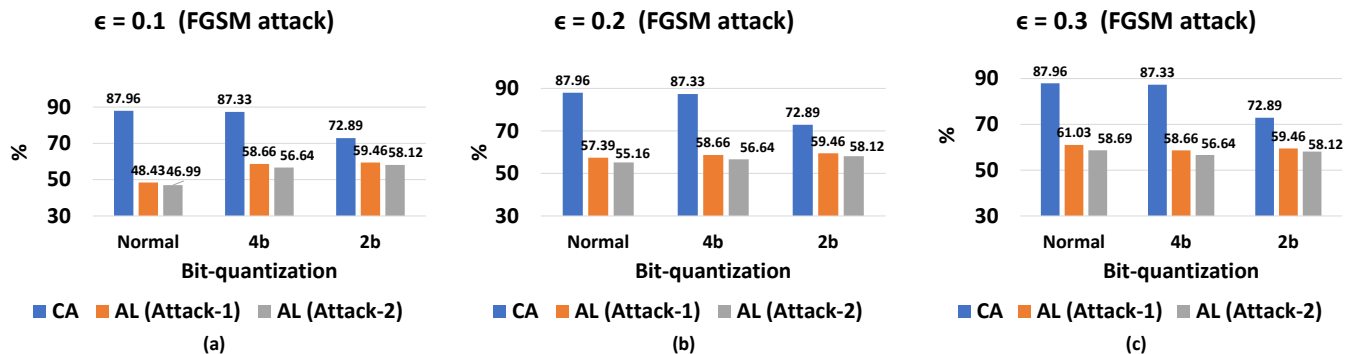


Fig. 11. Bar-diagram showing CAs and ALs (for FGSM-based *Attack-1* and *Attack-2*) for a VGG8 network mapped on 32x32 crossbars using CIFAR-10 dataset for different bit-discretizations of input pixels (4-bit and 2-bit) with - (a) $\epsilon = 0.1$; (b) $\epsilon = 0.2$; (c) $\epsilon = 0.3$

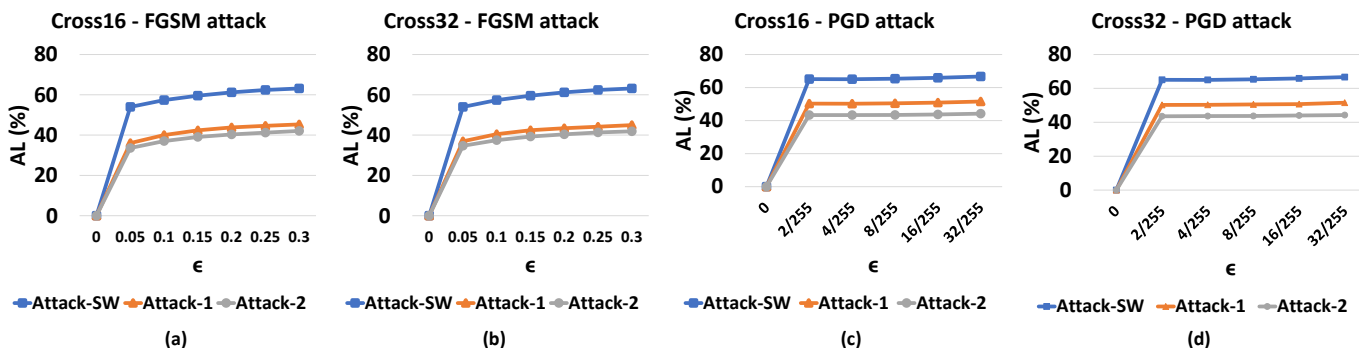


Fig. 12. (a)-(b) A plot between AL and ϵ for Attack-SW, Attack-1 and Attack-2 (FGSM) on Model-1 (VGG16 with CIFAR-100 dataset) for crossbar sizes 16x16 and 32x32 respectively; (c)-(d) A plot between AL and ϵ for Attack-SW, Attack-1 and Attack-2 (PGD) on Model-1 (VGG16 with CIFAR-100 dataset) for crossbar sizes 16x16 and 32x32 respectively

during adversarial attacks in case of DNNs mapped on crossbars than that of software-based DNNs ($> 10 - 15\%$). We also find that larger crossbar sizes extend greater resilience to the DNNs even against stronger PGD attacks.

We investigate the influence of various crossbar parameters on the adversarial robustness of the mapped DNNs. While large values of R_{MAX} do not produce any appreciable effect on adversarial robustness, a smaller value of R_{MIN} makes the network more adversarially robust. Furthermore, increasing the σ/μ ratio of the synaptic devices pertaining to process variation does not yield any significant benefit in terms of adversarial robustness. We further compare the performance of our non-ideality driven approach to adversarial robustness in a 32x32 crossbar with other state-of-the-art software-based adversarial defense techniques on CIFAR-100 dataset. We find that our approach performs significantly well in terms of reducing adversarial losses during FGSM or PGD attacks.

In our present work, in order to substantiate our claim, we have taken into account a crossbar system that does not include selector devices (such as MOSFETs) being connected in series with the resistive synaptic devices. In other words, we have not considered the impact of non-idealities pertaining to 1T-1R crossbar system that are non-linear in nature. Thus, in our future work we shall extend our analysis to 1T-1R memristive crossbar arrays by employing an architecture similar to *GENIE-x* [9] that accounts for both data-dependent and data-independent non-idealities while

modeling the crossbar instances. Finally, our comprehensive analysis and encouraging results establish the idea of re-thinking analog crossbar computing for adversarial security in addition to energy efficiency.

ACKNOWLEDGEMENT

This work was supported in part by the National Science Foundation (Grant#1947826), and the Amazon Research Award.

REFERENCES

- [1] Catherine D. Schuman et al. *A Survey of Neuromorphic Computing and Neural Networks in Hardware*. 2017. arXiv:1705.06963 [cs.NE].
- [2] H. -. P. Wong et al. MetalOxide RRAM. In: *Proceedings of the IEEE* 100.6 (2012), pp. 1951-1970.
- [3] Mrigank Sharad, Georgios D. Panagopoulos, and Kaushik Roy. Spinneuron for ultra low power computational hardware. In: *70th Device Research Conference* (2012), pp. 221-222.
- [4] Wei-Hao Chen et al. Circuit design for beyond von Neumann applications using emerging memory: From nonvolatile logics to neuromorphic computing. In: *18th International Symposium on Quality Electronic Design (ISQED)* (2017), pp. 2328.
- [5] A. Sengupta, Y. Shim, and K. Roy. Proposal for an All-Spin Artificial Neural Network: Emulating Neural and Synaptic Functionalities Through Domain Wall Motion in Ferromagnets. In: *IEEE Transactions on Biomedical Circuits and Systems* 10.6 (2016), pp. 1152-1160.
- [6] D. Fan et al. STT-SNN: A Spin-Transfer-Torque Based Soft-Limiting Non-Linear Neuron for Low-Power Artificial Neural Networks. In: *IEEE Transactions on Nanotechnology* 14.6 (2015), pp. 1013-1023.

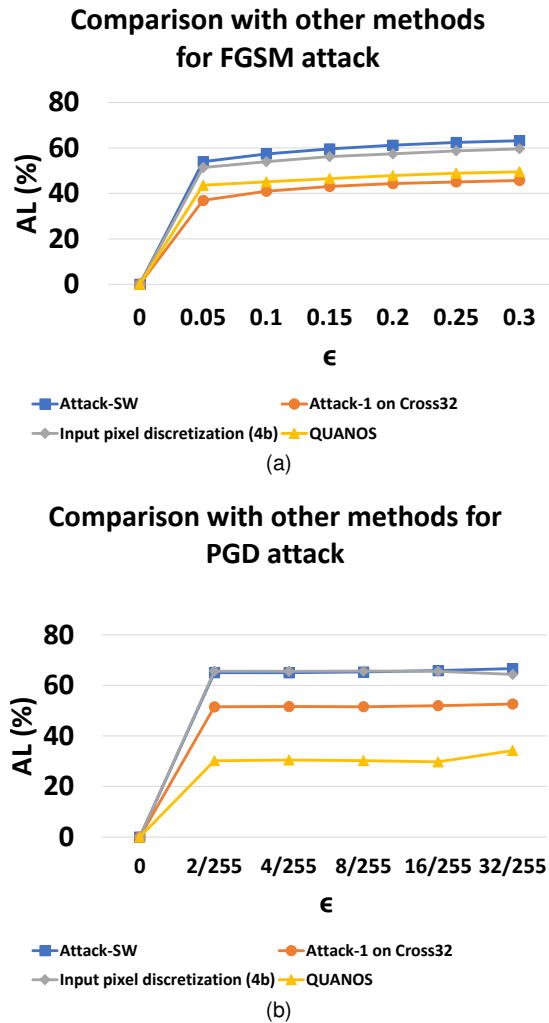


Fig. 13. (a) Comparison of our proposed method with other state-of-the-art adversarial defenses during FGSM attack using VGG16 network and CIFAR-100 dataset; (b) Comparison of our proposed method with other state-of-the-art adversarial defenses during PGD attack using VGG16 network and CIFAR-100 dataset

[7] Aayush Ankit et al. PUMA: A Programmable Ultra-efficient Memristor-based Accelerator for Machine Learning Inference. 2019. arXiv:1901.10351 [cs.ET].

[8] Shubham Jain et al. RxNN: A Framework for Evaluating Deep Neural Networks on Resistive Crossbars. 2018. arXiv:1809.00072 [cs.ET].

[9] Indranil Chakraborty et al. GENIE: A Generalized Approach to Emulating Non-Ideality in Memristive Xbars using Neural Networks. 2020. arXiv:2003.06902 [cs.ET].

[10] Shubham Jain and Anand Raghunathan. CxDNN: Hardware-Software Compensation Methods for Deep Neural Networks on Resistive Crossbar Systems. In: *ACM Trans. Embed. Comput. Syst.* 18.6 (Nov. 2019).

[11] Amogh Agrawal, Chankyu Lee, and Kaushik Roy. X-CHANGR: Changing Memristive Crossbar Mapping for Mitigating Line-Resistance Induced Accuracy Degradation in Deep Neural Networks. 2019. arXiv:1907.00285 [cs.ET].

[12] I. Chakraborty, D. Roy, and K. Roy. Technology Aware Training in Memristive Neuromorphic Systems for Nonideal Synaptic Crossbars. In: *IEEE Transactions on Emerging Topics in Computational Intelligence* 2.5 (2018), pp. 335344.

[13] Aleksander Madry et al. Towards Deep Learning Models Resistant to Adversarial Attacks. 2017. arXiv:1706.06083 [stat.ML].

[14] Nicholas Carlini et al. On Evaluating Adversarial Robustness. 2019. arXiv:1902.06705 [cs.LG].

[15] Priyadarshini Panda. QUANOS- Adversarial Noise Sensitivity Driven Hybrid Quantization of Neural Networks. 2020. arXiv:2004.11233 [cs.LG].

[16] Priyadarshini Panda, Indranil Chakraborty, and Kaushik Roy. Discretization Based Solutions for Secure Machine Learning Against Adversarial Attacks. In: *IEEE Access* 7 (2019), pp. 7015770168.

[17] Ji Lin, Chuang Gan, and Song Han. Defensive Quantization: When Efficiency Meets Robustness. 2019. arXiv:1904.08444 [cs.LG].

[18] Adam Paszke et al. Automatic differentiation in PyTorch. In: *NIPS-W*. 2017.

[19] Karen Simonyan and Andrew Zisserman. Very Deep Convolutional Networks for Large-Scale Image Recognition. 2014. arXiv:1409.1556 [cs.CV].

[20] Alex Krizhevsky. Learning multiple layers of features from tiny images. Tech. rep. 2009.

[21] Beiye Liu et al. Reduction and IR-drop compensations techniques for reliable neuromorphic computing systems. In: *IEEE/ACM International Conference on Computer-Aided Design (ICCAD)* (2014), pp. 6370.

[22] Aayush Ankit et al. Resparc: A reconfigurable and energy-efficient architecture with memristive crossbars for deep spiking neural networks. In: *Proceedings of the 54th Annual Design Automation Conference 2017*. 2017, pp. 16.

[23] Ali Shafiee et al. ISAAC: A convolutional neural network accelerator with in-situ analog arithmetic in crossbars. In: *ACM SIGARCH Computer Architecture News* 44.3 (2016), pp. 1426.

[24] Ping Chi et al. Prime: A novel processing-in-memory architecture for neural network computation in reRAM-based main memory. In: *ACM SIGARCH Computer Architecture News* 44.3 (2016), pp. 2739.

[25] Ian J. Goodfellow, Jonathon Shlens, and Christian Szegedy. Explaining and Harnessing Adversarial Examples. 2014. arXiv:1412.6572 [stat.ML].

[26] Alexey Kurakin, Ian Goodfellow, and Samy Bengio. Adversarial Machine Learning at Scale. 2016. arXiv:1611.01236 [cs.CV].

[27] Harini Kannan, Alexey Kurakin, and Ian Goodfellow. Adversarial Logit Pairing. 2018. arXiv:1803.06373 [cs.LG].

[28] Hyeungill Lee, Sungyeob Han, and Jungwoo Lee. Generative Adversarial Trainer: Defense to Adversarial Perturbations with GAN. 2017. arXiv:1705.03387 [cs.LG].

[29] Cihang Xie et al. Mitigating Adversarial Effects Through Randomization. 2017. arXiv:1711.01991 [cs.CV].

[30] Xuanqing Liu et al. Towards Robust Neural Networks via Random Self-ensembling. 2017. arXiv:1712.00673 [cs.LG].

[31] Gunet S. Dhillon et al. Stochastic Activation Pruning for Robust Adversarial Defense. 2018. arXiv:1803.01442 [cs.LG].

[32] Weilin Xu, David Evans, and Yanjun Qi. Feature Squeezing: Detecting Adversarial Examples in Deep Neural Networks. In: *Proceedings 2018 Network and Distributed System Security Symposium* (2018).

[33] Pouya Samangouei, Maya Kabkab, and Rama Chellappa. DefenseGAN: Protecting Classifiers Against Adversarial Attacks Using Generative Models. 2018. arXiv:1805.06605 [cs.CV].

[34] Dongyu Meng and Hao Chen. MagNet: a Two-Pronged Defense against Adversarial Examples. 2017. arXiv:1705.09064 [cs.CR].

[35] Fangzhou Liao et al. Defense against Adversarial Attacks Using High-Level Representation Guided Denoiser. 2017. arXiv:1712.02976 [cs.CV].

[36] Kui Ren et al. Adversarial Attacks and Defenses in Deep Learning. In: *Engineering* 6.3 (2020), pp. 346360.

[37] Aditi Raghunathan, Jacob Steinhardt, and Percy Liang. Certified Defenses against Adversarial Examples. 2018. arXiv:1801.09344 [cs.LG].

[38] Aman Sinha et al. Certifying Some Distributional Robustness with Principled Adversarial Training. 2017. arXiv:1710.10571 [stat.ML].

[39] Yiwen Guo et al. Sparse DNNs with Improved Adversarial Robustness. 2018. arXiv:1810.09619 [cs.LG].

[40] Xuanqing Liu et al. Adv-BNN: Improved Adversarial Defense through Robust Bayesian Neural Network. 2018. arXiv:1810.01279 [cs.LG].

[41] Nicolas Papernot et al. Practical Black-Box Attacks against Machine Learning. 2016. arXiv:1602.02697 [cs.CR].

[42] Zhezhi He et al. Noise Injection Adaption: End-to-End ReRAM Crossbar Non-ideal Effect Adaption for Neural Network Mapping. In: June 2019, pp. 16.